LES AND RANS STUDIES OF OSCILLATING FLOWS OVER FLAT PLATE

By Chin-Tsau Hsu,[1] Xiyun Lu,[2] and Man-Kim Kwan[3]

ABSTRACT: Oscillatory flows over a flat plate are studied by using Large Eddy Simulation (LES) and Reynolds-Average Navier-Stokes (RANS) methods. A dynamic subgrid scale (SGS) model is employed in LES, while the Saffman's turbulence model in RANS. The mean velocity profile, the turbulence intensity, and the wall shear stress are computed and compared with earlier experimental and numerical works. The results indicate that the flow behaviors are quite different during the accelerating and decelerating phases of the oscillating cycle. The transition from laminar to turbulent is also investigated as a function of the Reynolds number, R, which represents the square of the ratio of the oscillation amplitude at free stream to the thickness of the Stokes layer at the plate. The present results both from LES and RANS show that the transition occurs in the range of $5 \times 10^4 < R < 5 \times 10^5$. The evolution of the flow structure in the Stokes layer during the transition from laminar to turbulent is clearly demonstrated from the numerical results. The friction coefficient of the amplitude of oscillatory surface shear stress varies as $R^{-0.5}$ with a phase angle of 45° in laminar regime and transition to $R^{-0.23}$ with a phase angle of about 10° in turbulence regime. These variations in the surface shear stress with the Reynolds number are in excellent agreement with the earlier experimental results of Kamphuis and the numerical results of Blondeaux. The excellent agreement between the LES and RANS demonstrated that Saffman's turbulence model, as originally intended by Saffman, is applicable for unsteady flows.

INTRODUCTION

An oscillatory flow over a flat plate has its theoretical and practical significance. One relevant problem is the interaction between surface gravity waves and sea bottom for the understanding of wave damping and sediment transport in shallow waters. As the waves propagate from the generating area (usually deep water) towards the coast, the flow near the bottom develops into an oscillatory boundary layer and transition from laminar to turbulent. The characteristics of turbulence in such an oscillatory flow is quite different from that of wall turbulence in steady mean flow. Therefore, investigations are needed to understand the behaviors of oscillatory flows, such as the mean velocity profiles, the turbulence intensities, and the surface shear stress, especially during the accelerating and decelerating phases.

Although there were a few experimental investigations by Hino et al. (1983), Sato et al. (1987), and others, little numerical simulation works were done for oscillatory turbulent flows over a flat wall. Blondeaux (1987) studied numerically the turbulent Stokes layer generated by an oscillating flat plate of infinite extent in a fluid at rest by using the Reynolds-Average Navier-Stokes (RANS) method based on Saffman's (1970) turbulence model. However, he reported little information on the phase of flow oscillation, especially the oscillatory wall shear stress. As a result, there remain some open questions on the evolution of phase angle of the oscillatory flow in the Stokes layer during the transition from laminar to turbulence. More recently, large eddy simulation (LES) has been developed to become one of the most powerful computational tools available for the calculation of turbulent flows. Most of the LES works were done for studying flows with steady mean velocity of simple geometry (Galperin and Orszag 1993). Lu et al. (1997), however, employed LES method to calculate oscillating flows past a circular cylinder, which demonstrated the applicability of LES method to flows with unsteady mean velocity.

In this study, oscillatory flows over a flat plate are studied by using both LES and RANS methods. In LES method, the spatially filtered time-dependent three-dimensional incompressible Navier-Stokes equations were solved by using the non-staggered-grid, fractional time step scheme (Zang et al. 1994) and by employing a dynamic subgrid scale model of Germano et al. (1991). The advantage of adapting the Germano et al. (1991) dynamic subgrid scale model lays on the continuous update of eddy viscosity during simulation, which renders the model feasible for studying the flow transition. In RANS simulation, we employed Saffman's turbulence model (Saffman 1970; Saffman and Wilcox 1974) as that used by Blondeaux (1987). Therefore, the comparison to and the extension of Blondeaux's (1987) work can be adequately done. Another advantage of using Saffman's turbulence model is the model's capability to simulate both oscillatory laminar and turbulent flows as demonstrated by Blondeaux (1987). Therefore, the comparison of LES and RANS results becomes feasible.

Due to much cost and long real time required for LES, only three runs of different Reynolds numbers were computed in the present study. Hence, the results from LES were unable to cover a wide range of Reynolds number to reveal the detail on the evolution of the oscillating flows from laminar to turbulence. However, the LES can provide more details on the flow-fields at each Reynolds number. On the other end, it is relatively inexpensive to perform the RANS model, as many runs as required to cover a wide range of oscillating flows from laminar to turbulence. Therefore, a more complete picture of oscillating flows over a flat plate, especially the evolution of velocity and the wall shear stress during transition, can be delineated by RANS.

MATHEMATICAL FORMULATION

LES Formulation

The spatially filtered time-dependent three-dimensional incompressible Navier-Stokes equations as used for LES are given by

$$\frac{\partial \bar{u}_j}{\partial x_j} = 0 \tag{1}$$

$$\frac{\partial \bar{u}_j}{\partial t} + \frac{\partial}{\partial x_j}(\bar{u}_j \bar{u}_i) = -\frac{\partial \bar{p}}{\partial x_i} + \frac{\partial}{\partial x_j}\left(\nu \frac{\partial \bar{u}_i}{\partial x_j} - \tau_{ij}\right) \tag{2}$$

[1]Dept. of Mech. Engrg., Hong Kong Univ. of Sci. and Technol., Hong Kong.

[2]Dept. of Mech. Engrg., Hong Kong Univ. of Sci. and Technol., Hong Kong; Dept. of Modern Mech., Univ. of Sci. and Technol. of China, Hefei, Anhui 230026, China.

[3]Dept. of Mech. Engrg., Hong Kong Univ. of Sci. and Technol., Hong Kong.

Note. Associate Editor: Alexander Cheng. Discussion open until July 1, 2000. To extend the closing date one month, a written request must be filed with the ASCE Manager of Journals. The manuscript for this paper was submitted for review and possible publication on November 3, 1998. This paper is part of the ***Journal of Engineering Mechanics***, Vol. 126, No. 2, February, 2000. ©ASCE, ISSN 0733-9399/00/0002-0186–0193/$8.00 + $.50 per page. Paper No. 19575.

with $i, j = 1-3$, where $\bar{u}_i$ represents the filtered Cartesian velocities; $\bar{p}$ the filtered pressure divided by fluid density; ν the viscosity; and τ_{ij} the unresolved subgrid scale (SGS) stress term defined as

$$\tau_{ij} = \bar{u}_i \bar{u}_j - \bar{u}_i \bar{u}_j \tag{3}$$

These SGS quantities are modeled by using the dynamic subgrid scale eddy viscosity model (Germano et al. 1991; Zang et al. 1993). This is different from a classical eddy viscosity model (Smagorinsky 1963) for the subgrid scale stress which has a prescribed constant model coefficient. Instead, the dynamic SGS eddy viscosity model calculates the model coefficient using the resolved variables by filtering the governing equations at two different scales. This allows for the determination of the eddy viscosity dynamically to cover the range from laminar to turbulent. Therefore, the dynamic subgrid scale eddy viscosity model is most suitable for the investigation of flow transition (Piomelli and Zang 1991; Kleiser and Zang 1991).

To render an LES code applicable for various types of geometry, the code was constructed in a curvilinear coordinate system, ξ_m, $m = 1-3$ (Yuan et al. 1999). In simulating oscillating flows, here we use the velocity amplitude U_∞ and the displacement amplitude A_∞ of the flow oscillation at the free stream as the velocity and length scales, respectively. Note that $U_\infty = 2\pi f A_\infty$ with f being the frequency of the oscillation. Eqs. (1) and (2) are then transformed through the curvilinear coordinate system into the following nondimensional conservation equations:

$$\frac{\partial U_m}{\partial \xi_m} = 0 \tag{4}$$

$$\frac{\partial}{\partial t}(J^{-1}\bar{u}_i) + \frac{\partial}{\partial \xi_m}(U_m \bar{u}_i) = -\frac{\partial}{\partial \xi_m}\left(J^{-1}\frac{\partial \xi_m}{\partial x_i}\bar{p}\right) + \frac{\partial}{\partial \xi_m}\left[\left(\frac{1}{\mathrm{R}} + \frac{1}{\mathrm{R}_T}\right)\left(G^{mn}\frac{\partial \bar{u}_i}{\partial \xi_n}\right)\right] \tag{5}$$

where t = dimensionless time normalized by $1/2\pi f$; R = Reynolds number defined as $\mathrm{R} = 2\pi f A_\infty^2/\nu$; and R_T = Reynolds number of the turbulent eddy viscosity calculated from the dynamic subgrid scale eddy viscosity model (Germano et al. 1991; Zang et al. 1993). In (4) and (5), J^{-1} is the inverse of Jacobian, U_m is the contra-variant velocity along ξ_m multiplied by J^{-1}, and G^{mn} is the "mesh skewness tensor"; they are defined, respectively, by

$$J^{-1} = \det\left(\frac{\partial x_i}{\partial \xi_j}\right); \quad U_m = J^{-1}\frac{\partial \xi_m}{\partial x_j}\bar{u}_j; \quad G^{mn} = J^{-1}\frac{\partial \xi_m}{\partial x_j}\frac{\partial \xi_n}{\partial x_j} \tag{6a–c}$$

In the present calculation, we use periodic boundary conditions in streamwise and lateral directions and no-slip boundary condition on the plate surface. At upper boundary far away from the plate, nondimensional velocity along streamwise direction is set as $\bar{u}_\infty = \sin(t)$.

RANS Formulation

We define a Cartesian coordinate system (x, y, z), with the x-axis being along the flow oscillation direction lying on the plate and the y- and z-axes in the normal and lateral directions. By decomposing the velocity into an ensemble-averaged velocity (u v, w) and a turbulent fluctuation velocity (u', v', w'), the Reynolds-Average Navier-Stokes (RANS) equations reduce to the following simple one-dimensional form:

$$\frac{\partial u}{\partial t} = \frac{\partial}{\partial y}\left[\nu\frac{\partial u}{\partial y} - \langle u'v'\rangle\right] \tag{7}$$

where the symbol $\langle\ \rangle$ denotes the ensemble average. In order to close (7), Saffman's (1970) turbulence model for $\langle u'v'\rangle$ is used. In the Saffman's model, the Reynolds stress tensor is expressed in terms of an eddy viscosity ν_T and an averaged strain tensor, which for parallel mean flow reduces to

$$-\langle u'v'\rangle = \nu_T\frac{\partial u}{\partial y} \tag{8}$$

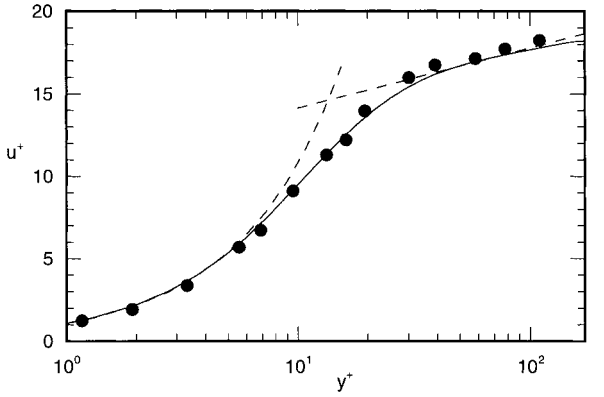

FIG. 1. Mean-Velocity in Wall Coordinates for Fully Developed Turbulent Channel Flow at R = 3,300, Computed by LES: —— = Computed Result; ● = Eckelmann (1974); – – – – – = Law of Wall

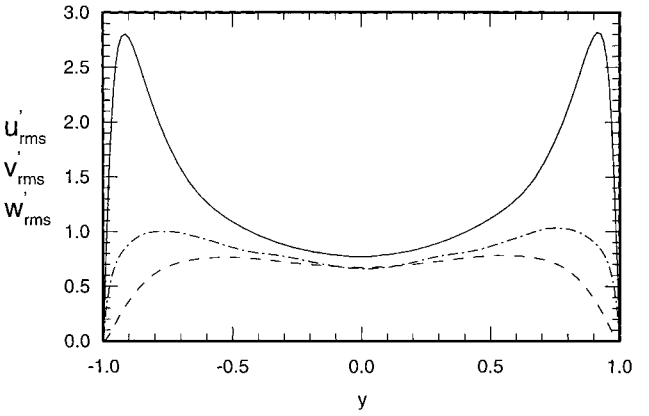

(a) in global coordinates

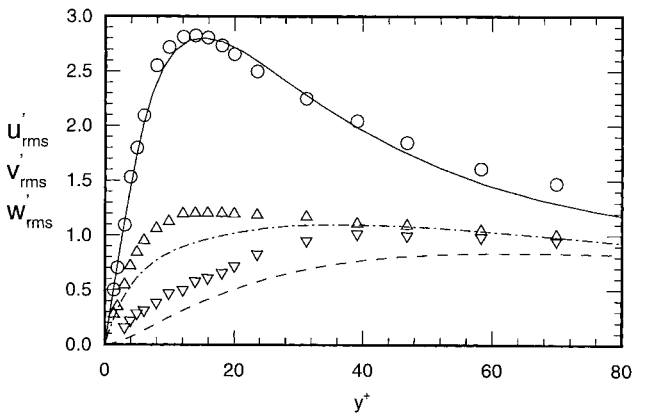

(b) in wall coordinates

FIG. 2. Resolvable Turbulence Intensities for Channel Flow at R = 3,300, Computed by LES. Computed Result: —— = u'_{rms}; – – – – – = v'_{rms}; – · – · – · – = w'_{rms}. Experimental Data of Kreplin and Eckelmann (1979): ○ = u'_{rms}; ▽ = v'_{rms}; △ = w'_{rms}

The eddy viscosity is assumed to be a function of local properties of turbulence, namely, a pseudo-energy e and a pseudo-vorticity ω, which satisfy, respectively, the following nonlinear diffusion equations:

$$\frac{\partial e}{\partial t} = \alpha_e e \left|\frac{\partial u}{\partial y}\right| - \beta_e e\omega + \frac{\partial}{\partial y}\left[(\nu + \sigma_e \nu_T)\frac{\partial e}{\partial y}\right] \quad (9)$$

$$\frac{\partial \omega^2}{\partial t} = \alpha_\omega \omega^2 \left|\frac{\partial u}{\partial y}\right| - \beta_\omega \omega^3 + \frac{\partial}{\partial y}\left[(\nu + \sigma_\omega \nu_\omega)\frac{\partial \omega^2}{\partial y}\right] \quad (10)$$

where α_e, α_ω, β_e, β_ω, σ_e, and σ_ω are assumed to be universal constants. A dimensional analysis of (9) and (10) leads to

$$\nu_T = \gamma \frac{e}{\omega} \quad (11)$$

where γ is another model constant. The values of these constants had been determined by Saffman and Wilcox (1974) on the basis of theoretical arguments. In the present computation, we followed Jacobs (1984) to use $\alpha_e = 0.3$, $\alpha_\omega = 0.18$, $\beta_e = 0.09$, $\beta_\omega = 0.15$, $\sigma_e = 0.5$, $\sigma_\omega = 0.5$, and $\gamma = 1.0$.

Substituting (8) and (11) into (7), (9), and (10), and using the length, velocity, and time scales as described in LES formulation, the nondimensional forms of the resultant equations become

$$\frac{\partial u}{\partial t} = \frac{\partial}{\partial y}\left[\left(\frac{1}{R} + \gamma \frac{e}{\omega}\right)\frac{\partial u}{\partial y}\right] \quad (12)$$

$$\frac{\partial e}{\partial t} = \alpha_e e \left|\frac{\partial u}{\partial y}\right| - \beta_e e\omega + \frac{\partial}{\partial y}\left[\left(\frac{1}{R} + \sigma_e \gamma \frac{e}{\omega}\right)\frac{\partial e}{\partial y}\right] \quad (13)$$

$$\frac{\partial \omega^2}{\partial t} = \alpha_\omega \omega^2 \left|\frac{\partial u}{\partial y}\right| - \beta_\omega \omega^3 + \frac{\partial}{\partial y}\left[\left(\frac{1}{R} + \sigma_\omega \gamma \frac{e}{\omega}\right)\frac{\partial \omega^2}{\partial y}\right] \quad (14)$$

The proper boundary conditions for (12)–(14) are

$$u = 0; \quad e = 0; \quad \omega = \frac{\alpha_e}{S}\left|\frac{\partial u}{\partial y}\right| \quad \text{at} \quad y = 0 \quad (15a\text{–}c)$$

and

$$u = u_\infty = \sin(t); \quad e \to 0; \quad \omega \to 0 \quad \text{at} \quad y \to \infty \quad (16a\text{–}c)$$

where S = a constant that takes the value of 100 according to Blondeaux (1987).

NUMERICAL PROCEDURE

Numerical solutions to the equation system (4) and (5) for LES are obtained by the non-staggered-grid, fractional step

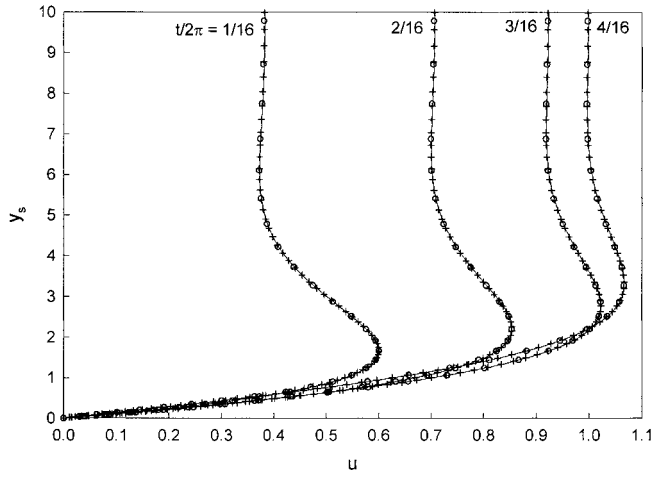

(a) acceleration phase

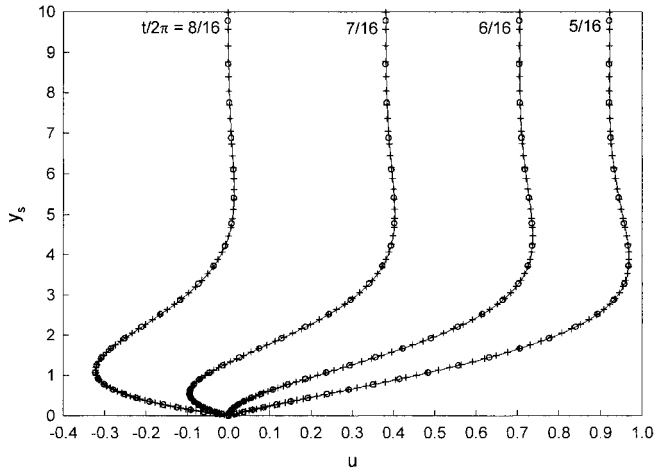

(b) deceleration phase

FIG. 3. Velocity Profiles during Half-Cycle of Oscillation as Predicted by RANS at R = 1,000. ○ = Number of Grids = 201, $\Delta t/2\pi = 0.0005$; + = Number of Grids = 401, $\Delta t/2\pi = 0.00025$; —— = Laminar Closed-Form Solution

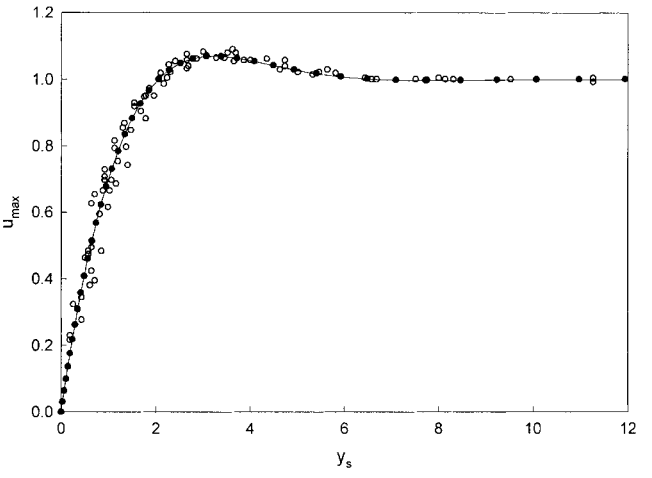

(a) amplitude of velocity

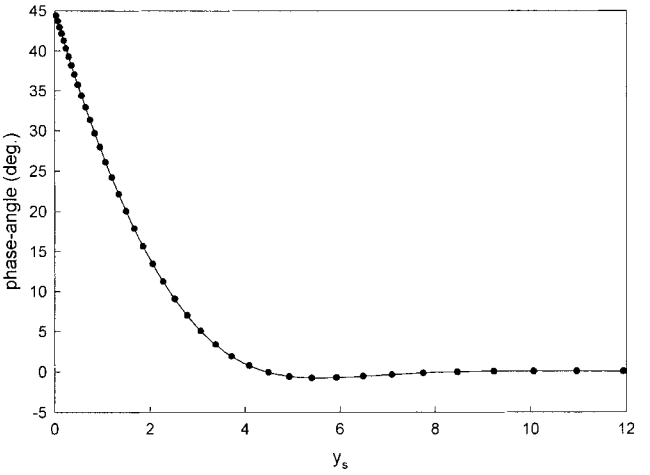

(b) phase-angle

FIG. 4. Amplitude and Phase-Angle Distributions of Oscillating Velocity as Predicted by RANS at R = 1,000. ● = Computed Result; ○ = Liu et al. (1996); —— = Laminar Closed-Form Solution

method. Following Zang et al. (1994), a semi-implicit time-advancement scheme is adopted with the Adams-Bashforth method for the explicit terms and the Crank-Nicolson method for the implicit terms. The discretized equations are

$$\frac{\delta U_m}{\delta \xi_m} = 0 \tag{17}$$

$$J^{-1}\frac{\bar{u}_i^{n+1} - \bar{u}_i^n}{\Delta t} = \frac{3}{2}\left[C_i^n + D_E(\bar{u}_i^n)\right] - \frac{1}{2}\left[C_i^{n-1} + D_E(\bar{u}_i^{n-1})\right] + R_i(\bar{p}^{n+1}) + \frac{1}{2}\left[D_I(\bar{u}_i^{n+1} + \bar{u}_i^n)\right] \tag{18}$$

where $\delta/\delta\xi_m$ represents discrete finite-difference operator in computational domain with the superscript being the time step and and the subscript the grid index. In (18), C_i is the convective term, R_i is the discrete operator for the pressure gradient terms, and D_E and D_I are the discrete operators for the explicitly treated off-diagonal viscous terms and the implicitly treated diagonal viscous terms, respectively. These terms have the following forms:

$$C_i = -\frac{\delta}{\delta \xi_m}(U_m \bar{u}_i); \quad R_i = -\frac{\delta}{\delta \xi_m}\left(J^{-1}\frac{\delta \xi_m}{\delta x_i}\right) \tag{19a,b}$$

$$D_I = \frac{\delta}{\delta \xi_m}\left[\left(\frac{1}{\mathrm{R}} + \frac{1}{\mathrm{R}_T}\right) G^{mn}\frac{\delta}{\delta \xi_n}\right], \quad m = n \tag{20a}$$

$$D_E = \frac{\delta}{\delta \xi_m}\left[\left(\frac{1}{\mathrm{R}} + \frac{1}{\mathrm{R}_T}\right) G^{mn}\frac{\delta}{\delta \xi_n}\right], \quad m \neq n \tag{20b}$$

Except for the convective terms, all the spatial derivatives are approximated with second-order center differences. The convective terms are discretized by a variation of QUICK scheme given in Perng and Street (1989). Using the fractional step method, the time advancement in (18) is solved with a predictor-corrector solution procedure. The pressure is then obtained by solving the pressure Poisson's equation using the multigrid method (Perng and Street 1989). In comparison to LES, the numerical procedure for RANS is relatively simple. However, the spatial derivatives in (12)–(14) of RANS formulation are discretized using a central difference scheme, while the time derivative is discretized by a second-order Adams-Bashforth scheme.

In the present computation, the number of mesh points for LES calculations was 65 × 65 × 65 in streamwise, spanwise, and wall-normal directions, respectively, with a time step of 0.001. The computational grid is nonuniform in the wall normal direction, but is uniform in the streamwise and spanwise directions. In order to increase the resolution of mesh near the wall, stretching transformation is used along the wall-normal direction. This mesh number is comparable to those used by Zang et al. (1993) with 64 × 64 × 32 and by Germano et al. (1991) with 48 × 65 × 64. They also demonstrated the adequacy of using such mesh points by examining the dependency of the LES code on the mesh size. As our LES code is inherent from the Stanford's LES code and the Reynolds numbers of this study are of the same order as those of Germano et al. (1991) and Zang et al. (1993), it is anticipated that the mesh size used in the present calculation is adequate. This LES mesh number is also the maximum number that can be handled by our current computing power. The mesh number for RANS was 201 in wall-normal direction with a time step of 0.0005. Again, the mesh was stretched along the wall-normal direction to increase the resolution near the wall. As to be shown later, the computed results are verified to be independent of the time steps and the grid sizes.

The LES and RANS codes were executed with prescribed initial condition and the results were extracted after the code had been executed for more than 10 oscillation periods, when the periodically oscillatory flow has reached a steady state, i.e., when the initial transient effect becomes negligible.

CODE VALIDATION

To validate the LES code, we first calculated a fully developed turbulent channel flow at R = 3,300, based on the mean centerline velocity and channel half-width, using a grid number of 65 × 65 × 65 in the streamwise, spanwise, and wall-normal directions and a time step of 0.001. The mean velocity profile is calculated by taking time average and then spatial average over x–z-planes (homogeneous directions). The mean

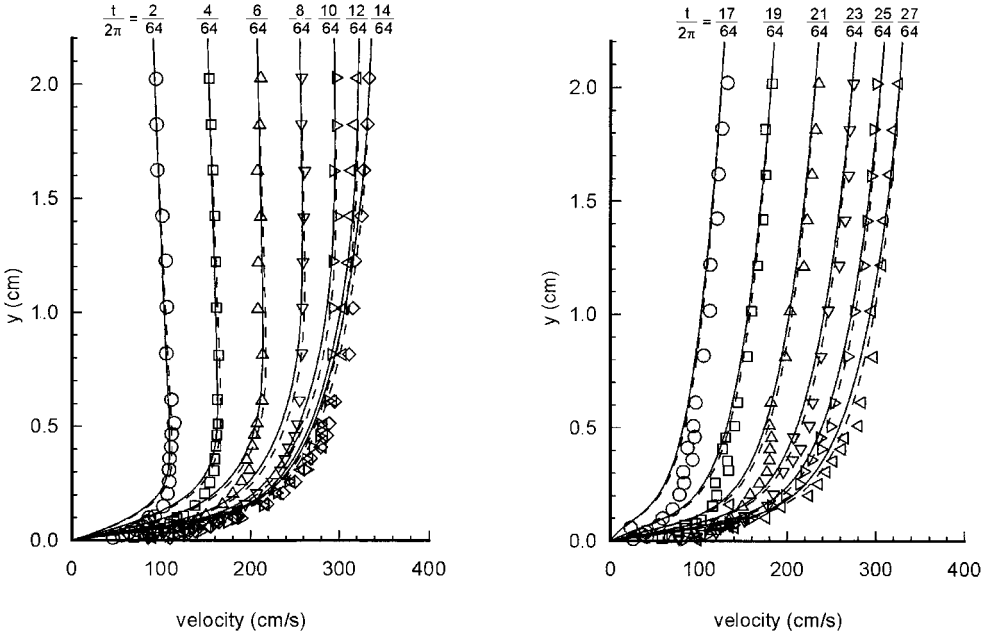

(a) acceleration phase (b) deceleration phase

FIG. 5. Velocity Profiles Predicted by RANS at R = 4 × 10^5 at Different Phases during Half Oscillating Cycle: —— = Number of Grids = 201, $\Delta t/2\pi$ = 0.0005; – – – – – , Number of Grids = 401, $\Delta t/2\pi$ = 0.00025 [Symbols, Hino et al. (1983)]

velocity profile in terms of wall coordinate (u^+, y^+) as normalized by the friction velocity u_* and the viscous sublayer thickness ν/u_* is shown in Fig. 1. Also shown in Fig. 1 are the experimental data obtained by Eckelmann (1974). The two dashed lines represent the linear law and the semilog law of the wall. Within the viscous sublayer, $y^+ < 5$, both the experimental and computational results follow the linear law of the wall. For $y^+ > 40$, the computed mean-velocity profile shows the semilogarithmic relation and is in good agreement with the experimental results. From the mean velocity profile, the Reynolds number, based on the friction velocity and channel half-width, is $R_\tau = 180$, which is in excellent agreement with the DNS result by Kim et al. (1987). The turbulence intensities normalized by the friction velocity are shown in Fig. 2(a), and their close-up near the wall in terms of wall coordinate y^+ are shown in Fig. 2(b). The comparison of the present calculated results with the experimental data by Kreplin and Eckelmann (1979) at Reynolds number $R_\tau = 194$ shows that they are in good agreement.

To validate the RANS code, we implement the code directly to the problem of oscillating flows over the flat plate at the Reynolds number equals to 1,000, which is below the transition. If the RANS code performs adequately, it will automatically yield the solution for laminar oscillating flow, which has an exact closed-form solution given in real form by

$$u = \sin t - \exp\left(-\frac{y_s}{\sqrt{2}}\right)\sin\left(t - \frac{y_s}{\sqrt{2}}\right) \qquad (21)$$

where $y_s = y(R)^{1/2}$ represents the dimensionless coordinate normalized by the Stokes layer thickness $\delta_s = (\nu/2\pi f)^{1/2}$. The validation results are given in the next section when the numerical results of RANS simulation are presented.

RESULTS AND DISCUSSION

RANS Results

Fig. 3 shows the RANS predictions of the oscillatory velocity profiles during the acceleration [Fig. 3(a)] and deceleration [Fig. 3(b)] phases of the half-cycle oscillation at $R = 1{,}000$. Two sets of RANS results for different mesh numbers of 201 and 401 and different time steps of $\Delta t/2\pi = 0.0005$ and 0.00025, respectively, are presented in Fig. 3. For comparison the exact close solution calculated from (21) is also plotted as the solid-line curve in Fig. 3. From Fig. 3, it is clear that the RANS model based on Saffman's turbulence closure predicts excellently the laminar oscillating flows. The results shown in Fig. 3 also indicate that the RANS code is independent of the mesh size and time step used in the present study if the oscillating flow is laminar. For a better understanding of the flow structure, the oscillatory velocity profiles are plotted as the distributions of amplitude and phase-angle as shown in Fig. 4 and compared with the experimental data obtained recently by Liu et al. (1996). Only amplitude data of Liu et al. (1996) were plotted in Fig. 4 since they did not report the data of phase-angle distribution. Hereafter, the phase-angle refers as the phase lead to the phase-angle of velocity oscillation in free stream. Excellent agreement is found among the RANS predictions, the closed-form results and the experimental data.

With the above code validation, the RANS code is then executed for oscillating flows at higher Reynolds number. The case at $R = 4 \times 10^5$ was simulated since it corresponds to one experimental run of Hino et al. (1983). To examine the dependence of code on mesh size and time step on oscillating turbulent flows, two sets of numerical results for different mesh sizes and time steps as in laminar flow case are computed. Fig. 5 shows the velocity profiles as predicted by the RANS method during the acceleration [Fig. 5(a)] and deceleration [Fig. 5(b)] phases of the half-cycle. To plot the experimental data of Hino et al. (1983) for comparison, the profiles in Fig. 5 are presented in dimensional form. From Fig. 5, it is seen that the accuracy of numerical results due to different mesh sizes and the time steps is within an acceptable level of 5%. Good agreements between the predictions and the experimental data are also found in Fig. 5.

Fig. 6 shows the profiles of amplitude [Fig. 6(a)] and phase-angle [Fig. 6(b)] of velocity oscillation at $R = 10^3$, 10^5, and 10^6. As to be seen later, they correspond to the cases of laminar, transition, and turbulent oscillatory flows. The evolution of the oscillatory flow structure from laminar to turbulent is clearly demonstrated in Fig. 6. The effect of turbulence apparently has increased the shear stress at the wall and thickened the Stokes layer. Turbulence also reduces the phase lead of the oscillation in the Stokes layer to that in the free stream. Fig. 6 clearly shows that the oscillating flows are indeed scaled with the Stokes layer thickness δ_s, but not the free stream oscillation amplitude A_∞.

LES Results

The mean velocity profiles obtained by space-averaging over the x, z-plane parallel to the wall, as calculated by LES

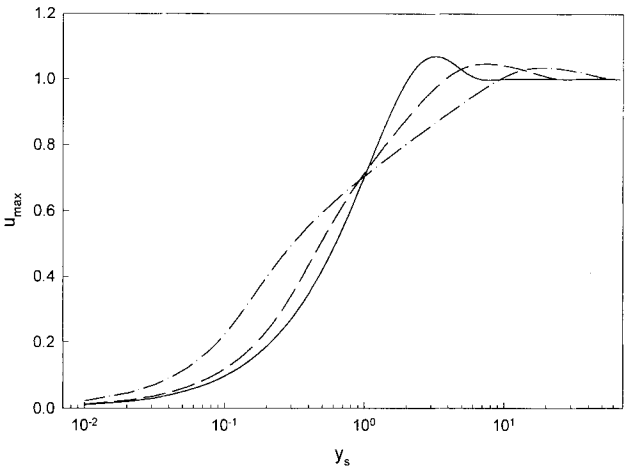

(a) amplitude of velocity

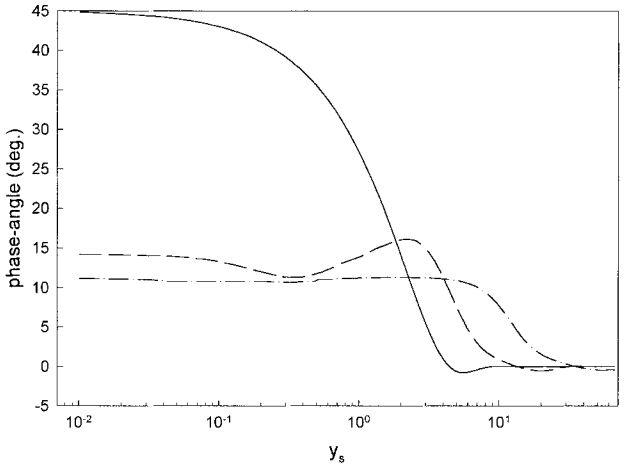

(b) phase-angle

FIG. 6. Amplitude and Phase-Angle Distributions of Oscillating Velocity as Predicted by RANS at Different R to Signify Difference among Laminar, Transition, and Turbulent Stokes Layers: ——, $R = 1 \times 10^3$; – – – – –, $R = 1 \times 10^5$; –·–·–·–·–, $R = 1 \times 10^6$

method at $R = 4 \times 10^5$, are plotted in Fig. 7 for the acceleration [Fig. 7(a)] and deceleration [Fig. 7(b)] phases of oscillation. For comparison, the numerical results as obtained by the RANS code are also plotted in Fig. 7. It is seen that the LES and RANS results agree very well. During the oscillation cycle, a layer that obeys the semilogarithmic law exists above the viscous sublayer where the velocity increases linearly from the wall. These phenomena are similar to those of the turbulent boundary layer of steady turbulent flows. However, the semilog law regions in the accelerating phase are narrower and closer to the wall, while those in the decelerating phase are broader and more far away from the wall. This behavior reveals the difference in turbulence characteristics between the accelerating and decelerating phase. This difference is also confirmed by the experimental results of Hino et al. (1983).

Fig. 8 shows the x, z-plane space-averaged turbulence intensities calculated by LES at $R = 4 \times 10^5$ during the acceleration (solid curves) and deceleration (dashed curves) phases. The intensity of u'_{rms} [Fig. 8(a)] near the wall in the streamwise direction is generally one order higher than those of other two components v'_{rms} [Fig. 8(b)] and w'_{rms} [Fig. 8(c)] in the wall-normal and spanwise directions, a behavior similar to that of a steady turbulent flow as shown in Fig. 2(b). However, the maximum values of u'_{rms} in the decelerating phase are higher than those in accelerating phase, i.e., turbulence is generated during deceleration and suppressed during acceleration.

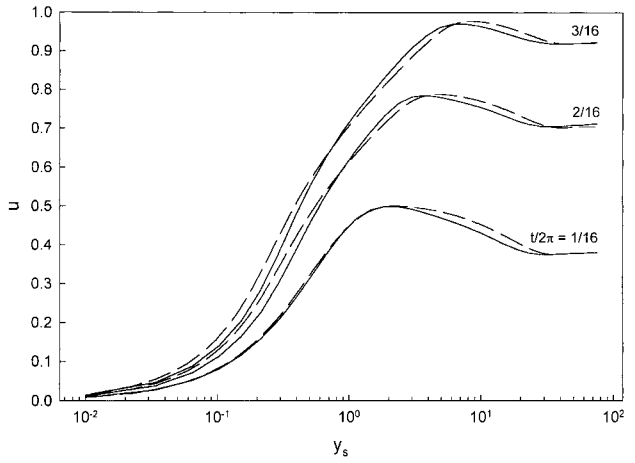

(a) acceleration phase

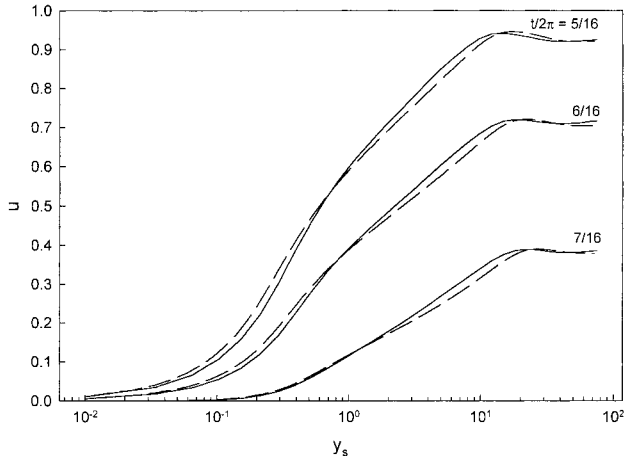

(b) deceleration phase

FIG. 7. *x-z* Plane Space-Averaged Velocity Profiles Calculated by LES at $R = 4 \times 10^5$: —— = LES; – – – – – = RANS

Wall Shear Stress

Fig. 9 shows the oscillations of the wall shear stress with time, as calculated by LES, RANS, and laminar prediction, respectively, at $R = 4 \times 10^5$. Here the wall shear stress τ_w is

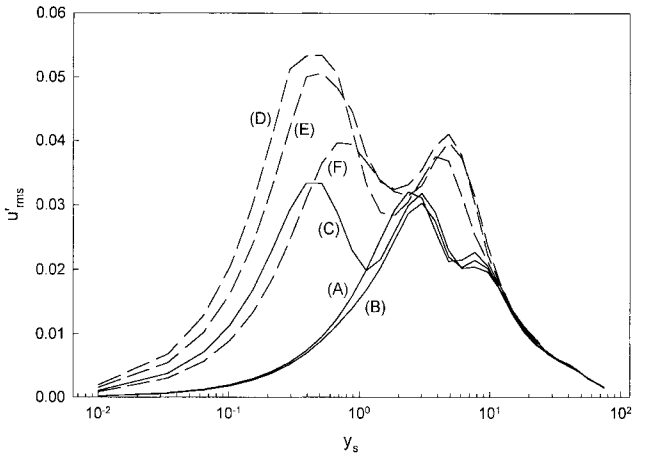

(a) stream-wise intensity

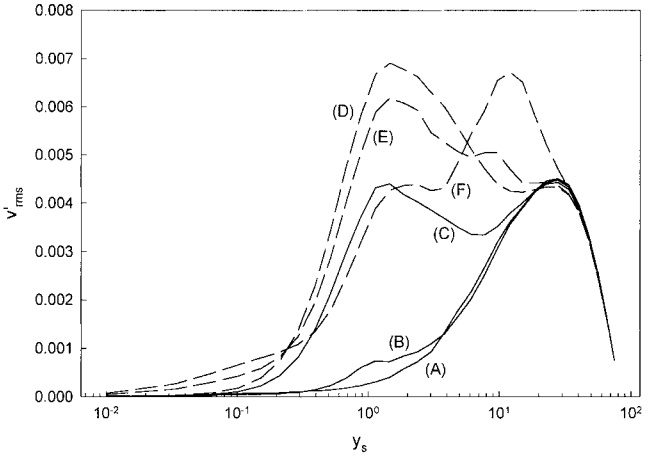

(b) wall-normal intensity

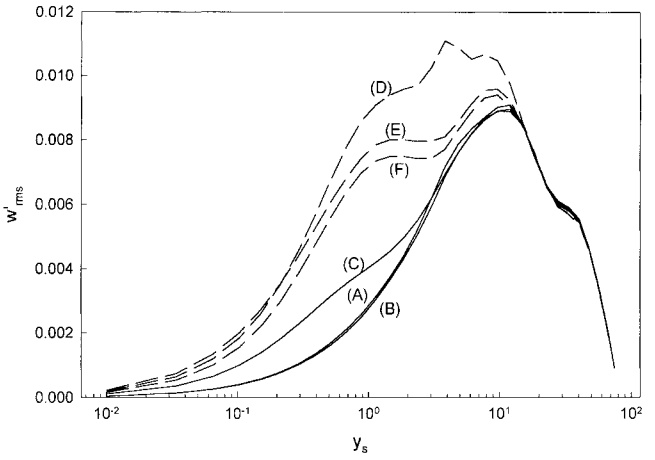

(c) span-wise intensity

FIG. 8. *x-z* Plane Space-Averaged Profiles of Resolvable Turbulence Intensities Calculated by LES at $R = 4 \times 10^5$ at Different Phases when $t/2\pi$ Equals: (A) 1/16; (B) 2/16; (C) 3/16; (D) 5/16; (E) 6/16; and (F) 7/16 (—— = Acceleration Phase; – – – – – = Deceleration Phase)

calculated by taking the y-derivative of the velocity profile at the wall, i.e., $\tau_w = \mu(\partial u/\partial y)_w$ and then expressed in term of the friction coefficient $C_F = \tau_w/\rho U_\infty^2$. It is seen from Fig. 9 that the results of LES and RANS are in very good agreement in terms of both amplitude and phase angle. The phase angle of the surface shear stress for the turbulent oscillating flow however is quite different from that of the laminar one, with a phase lag of about 35°. The amplitude of surface shear stress oscillation for turbulent oscillating flows is also observed to be higher than the laminar prediction by about 30%.

The variations of the surface shear stress as a function of the Reynolds number, as calculated by RANS and LES methods, are shown in Figs. 10 and 11, in terms of the amplitude and phase angle, respectively. For comparison, the experimental data of Kamphuis (1975) are also plotted in Fig. 10. It is observed that the present calculated results are in good agreement with the experimental data of Kamphuis (1975), except for the minor discrepancy in the transition regime. In Fig. 10, the two lines represent the friction coefficients in laminar regime, $C_{F\max} = 2R^{-0.5}$ as calculated by the analytic formula and in turbulent regime, $C_{F\max} = 0.1R^{-0.23}$ according to Blondeaux (1987). Excellent agreements among the theory, experiment, and computation are found in Fig. 10. However, the comparison is incomplete since the no phase-angle data were reported by Kamphuis (1975), nor Blondeaux (1987). To complete the characterization of surface shear stress, the variation of the phase angle with the Reynolds number is presented in Fig. 11. From Fig. 11, the transition from laminar to turbulent is clearly identified as to occur in the range of $5 \times 10^4 < R < 5 \times 10^5$. The phase angle is 45° in laminar regime, which decreases to about 10° in turbulent regime. The excellent agreement between the LES and RANS results is also found in Fig. 11.

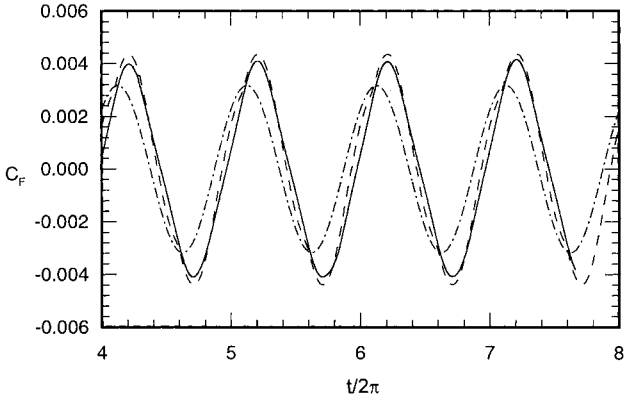

FIG. 9. Time-Varying Surface Shear Stress at R = 4 × 10⁵, as Expressed in Terms of Friction Coefficient C_F: – – – – – = RANS; —— = LES; – · – · – · – · – = Laminar Solution

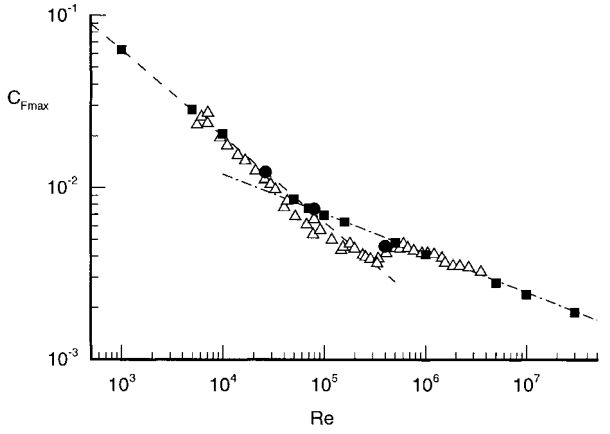

FIG. 10. Amplitude of Friction Coefficient C_{Fmax} versus Reynolds Number R: ■ = RANS; ● = LES; △ = Kamphuis (1975); – · – · – · – · – = Blondeaux (1987); – – – – – = Laminar Solution

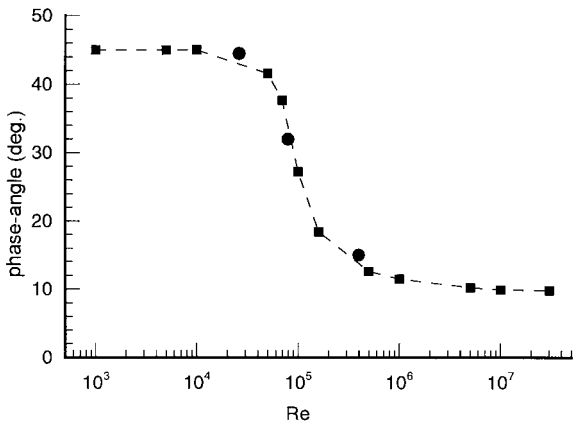

FIG. 11. Phase-Angle of Friction Coefficient versus Reynolds Number R: – – ■ – – = RANS; ● = LES

CONCLUDING REMARKS

Oscillatory flows over a flat plate area studied by LES and RANS methods for the Reynolds numbers ranging from laminar to turbulence regime. In LES, the spatially filtered time-dependent three-dimensional incompressible Navier-Stokes equations are solved using the non-staggered-grid, fractional step method, coupled with a dynamic subgrid-scale model. In RANS, the Reynolds-averaged Navier-Stokes equations are calculated with the Saffman's turbulence model. Based on our calculated results from both LES and RANS methods, the completely different features of turbulence structures, in term of viscous sublayer and the semilogarithmic profile, between the accelerating and decelerating phases can be identified. The variations of the amplitude and phase angle of the oscillatory surface shear stress with Reynolds numbers are also investigated. Excellent agreement among theoretical prediction, experimental data and the LES and RANS computations are found. The shifting of the phase angle from 45° to about 10° clearly identifies the transition from laminar to turbulent regime in the range of $5 \times 10^4 < R < 5 \times 10^5$. These excellent agreements between LES and RANS results in the oscillating flow structures as well as the wall shear stress suggest that Saffman's (1970) turbulence model is applicable for unsteady flows.

ACKNOWLEDGMENTS

The writers sincerely thank Prof. R. L. Street of Stanford University for providing the initial version of the LES code. This work is supported by the Hong Kong Government under RGC Grant Nos. HKUST708/95E and HKUST815/96E, and under RIG Grant No. R195/96.EG15.

APPENDIX. REFERENCES

Blondeaux, P. (1987). ''Turbulent boundary layer at the bottom of gravity waves.'' *J. Hydro. Res.*, 25, 447–461.

Eckelmann, H. (1974). ''The structure of the viscous sublayer and the adjacent wall region in a turbulent channel flow.'' *J. Fluid Mech.*, Cambridge, U.K., 65, 439.

Galperin, B., and Orszag, S. A. (1993). *Large eddy simulation of complex engineering and geophysical flows*. Cambridge University Press, Cambridge, U.K.

Germano, M., Piomelli, U., Moin, P., and Cabot, W. H. (1991). ''A dynamic subgrid-scale eddy viscosity model.'' *Phys. Fluids*, 3, 1760–1765.

Hino, M., Kashiwayanagi, M., Nakayama, A., and Hara, T. (1983). ''Experiments on the turbulence statistics and the structure of a reciprocating oscillatory flow.'' *J. Fluid Mech.*, Cambridge, U.K., 131, 363–400.

Jacobs, S. J. (1984). ''Mass transport in a turbulent boundary layer under a progressive water wave.'' *J. Fluid Mech.*, Cambridge, U.K., 146, 303–312.
Kamphuis, J. W. (1975). ''Friction factor under oscillatory waves.'' *J. Wtrwy., Harb. and Coast. Engrg. Div.*, ASCE, 101, 135.
Kim, J., Moin, P., and Moser, R. (1987). ''Turbulence statistics in fully developed channel flow at low Reynolds number.'' *J. Fluid Mech.*, Cambridge, U.K., 177, 133–166.
Kleiser, L., and Zang, T. A. (1991). ''Numerical simulation of transition in wall-bounded shear flows.'' *Ann. Rev. Fluid Mech.*, 23, 495–537.
Kreplin, H., and Eckelmann, H. (1979). ''Behavior of the three fluctuating velocity components in the wall region of a turbulent channel flow.'' *Phys. Fluids*, 22, 1233.
Liu, P. L.-F., Davis, M. H., and Downing S. (1996). ''Wave-induced boundary layer flows above and in a permeable bed.'' *J. Fluid Mech.*, Cambridge, U.K., 325, 195–218.
Lu, X. Y., Dalton, C., and Zhang, J. (1997). ''Application of large eddy simulation to an oscillating flow past a circular cylinder.'' *J. Fluids Engrg.*, 119, 519–525.
Perng, C.-Y., and Street, R. L. (1989). ''Three-dimensional unsteady flow simulations: alternative strategies for a volume-averaged calculation.'' *Int. J. Numer. Methods Fluids*, 9, 341–362.
Piomelli, U., and Zang, T. A. (1991). ''Large-eddy simulation of transitional channel flow.'' *Comp. Phys. Comm.*, 65, 224–230.
Saffman, P. G. (1970). ''A model for inhomogeneous turbulent flow.'' *Proc. Roy. Soc. London A*, 317, 417–433.
Saffman, P. G., and Wilcox, P. C. (1974). ''Turbulence model predictions for turbulent boundary layers.'' *AIAA J.*, 12, 541–546.
Sato, S., Shimosako, K., and Watanabe, A. (1987). ''Measurements of oscillatory turbulent boundary layer flow above ripples with a laser-Doppler velocimeter.'' *Coast. Engrg. in Japan*, Tokyo, 30, 89–98.
Smagorinsky, J. (1963). ''General circulation experiments with the primitive equations, I. The basic experiment.'' *Mon. Weather Rev.*, 91, 99–164.
Yuan, L. L., Street, R. L., and Ferziger, J. H. (1999). ''Large eddy simulations of a round jet in a crossflow.'' *J. Fluid Mech.*, Cambridge, U.K., 379, 71–104.
Zang, Y., Street, R. L., and Koseff, J. R. (1993). ''A dynamic mixed subgrid-scale model and its application to turbulent recirculating flows.'' *Phys. Fluids*, 5, 3186–3196.
Zang, Y., Street, R. L., and Koseff, J. R. (1994). ''A non-staggered grid, fractional step method for time-dependent imcompressible Navier-Stokes equations in curvilinear coordinates.'' *J. Comp. Phys.*, 114, 18–33.